Tomography of a Number-Resolving Detector by Reconstruction of an Atomic Many-Body Quantum State

Mareike Hetzel,[1,*] Luca Pezzè,[2] Cebrail Pür,[1] Martin Quensen,[1] Andreas Hüper,[1] Jiao Geng,[3,4] Jens Kruse,[1] Luis Santos,[5] Wolfgang Ertmer,[1] Augusto Smerzi,[2] and Carsten Klempt[1]

[1]*Institut für Quantenoptik, Leibniz Universität Hannover, Welfengarten 1, D-30167 Hannover, Germany*
[2]*QSTAR and INO-CNR and LENS, Largo Enrico Fermi 2, 50125 Firenze, Italy*
[3]*Key Laboratory of 3D Micro/Nano Fabrication and Characterization of Zhejiang Province, School of Engineering, Westlake University, 18 Shilongshan Road, Hangzhou 310024, Zhejiang Province, China*
[4]*Institute of Advanced Technology, Westlake Institute for Advanced Study, 18 Shilongshan Road, Hangzhou 310024, Zhejiang Province, China*
[5]*Institut für Theoretische Physik, Leibniz Universität Hannover, Appelstraße 2, D-30167 Hannover, Germany*

(Received 1 July 2022; accepted 10 October 2023; published 26 December 2023)

The high-fidelity analysis of many-body quantum states of indistinguishable atoms requires the accurate counting of atoms. Here we report the tomographic reconstruction of an atom-number-resolving detector. The tomography is performed with an ultracold rubidium ensemble that is prepared in a coherent spin state by driving a Rabi coupling between the two hyperfine clock levels. The coupling is followed by counting the occupation number in one level. We characterize the fidelity of our detector and show that a negative-valued Wigner function is associated with it. Our results offer an exciting perspective for the high-fidelity reconstruction of entangled states and can be applied for a future demonstration of Heisenberg-limited atom interferometry.

DOI: 10.1103/PhysRevLett.131.260601

High-fidelity preparation, manipulation, and detection of quantum states of many indistinguishable atoms have been greatly improved during the last decades. These facilitate exciting developments, from fundamental quantum atom optics [1,2] to entanglement-enhanced metrology [3]. Entangled states serve as highly sensitive input states of atom interferometers, reducing the resolution limit from the standard quantum limit (SQL) to the Heisenberg limit [4]. Applications range from interferometry [5–14] and magnetometry [15–18] to atomic clocks [19–22] and inertial sensing [23,24]. To date, atom counting noise represents one of the crucial limitations in current experiments, affecting fundamental studies and applications.

Recent experiments creating entangled atomic quantum states in ensembles of indistinguishable atoms have reported counting noise that ranges from 3 atoms at a total number of 600 atoms [25], to 1.6 atoms at 3000 atoms [26], to 10 atoms at 10^4 [27,28], to better than 17 atoms at 10^5 [14], and to 50 atoms at 5×10^5 [11]. Reducing the counting noise below the single atom level, where the quantization of the atomic signal becomes apparent, promises relevant improvement. For example, such a counting resolution would allow for the direct detection of Bell correlations between two separated atomic ensembles [29] and the observation of parity signals in Hong-Ou-Mandel-ike interference experiments with many-particle states [30,31]. In atom interferometry, number-resolving counting (NRC) can be applied to demonstrate a Heisenberg-limited resolution [32,33]. NRC has been obtained in a cavity-based detection [34], while restricted to a discrimination between 0 and 1, the scaling to larger numbers is an open challenge. Single-atom resolved detection has also been obtained in free-falling clouds [35–39], and was applied to extract correlations and entanglement. NRC for up to 1000 atoms has been demonstrated in a millimeter-sized magneto-optical trap (mMOT) [40,41], but was not applied to the detection of many-body quantum states.

The fine calibration of quantum measurement devices generally requires quantum detection tomography (QDT) techniques [42,43]. QDT provides a set of positive-operator-valued measures (POVM) that fully characterize the detector. So far, QDT has been mainly investigated for optical photocounting and homodyne detection [44–48] and also applied to characterize qubit readout for pairs of trapped ions [49] and quantum computing machines [50], but its potential has not yet been leveraged for the characterization of neutral-atom quantum systems.

In this Letter, we apply a MOT-based number counting [51] to analyze a simple dynamical evolution of a many-body spin state with single-atom resolution. We generate an atomic Bose-Einstein condensate (BEC) in one atomic clock level, apply a microwave (MW) coupling pulse of variable duration on the atomic clock transition, and count the number of atoms in the other, initially empty, level. Rabi dynamics is used to perform QDT. In particular, we are able to follow the time evolution of the coherent spin

state with a clear resolution of the number quantization. The number assignment fidelity of the detector is larger than 99.0% for up to 15 atoms, and is reduced to 72.3% when a specific spin level is selected. By applying a stochastic matrix approach to the recorded histograms, we obtain a set of nonclassical POVM operators that fully characterize the detection process. The expected Poissonian distributions are reproduced with a statistics-limited fidelity of up to 99%. We predict that the single-level detection operates an interferometric measurement with sub-SQL sensitivity using spin-squeezed states and monitoring a low-populated output. This Letter is a first step forward toward the detection, characterization, and application of entangled many-body quantum states with high-fidelity NRC.

We generate a BEC of 10^5 ^{87}Rb atoms in a crossed-beam optical dipole trap (ODT) with a preparation time of 3.3 s; see Ref. [52] for details on the BEC production. We prepare the BEC in the hyperfine level $|F, m_F\rangle = |2, 2\rangle$ and reduce the number of atoms to enter the regime of our number-resolved counting. This is realized by transferring 34 atoms to the level $|1, 1\rangle$, on average, and a subsequent optical removal of the residual atoms in the $F = 2$ manifold. A further MW pulse transfers the remaining atoms to the level $|2, 0\rangle$. A final resonant light push on the $F = 1$ manifold terminates our state preparation with 34 and 0 atoms in the clock states $|2, 0\rangle$ and $|1, 0\rangle$, respectively. The total number of particles fluctuates by 6.4 atoms, dominated by projection noise (5.8 atoms).

We apply a resonant MW pulse on the clock transition with a variable duration ranging from $t = 2.5$ to 56 μs. The many-body state in the pseudospin-1/2 system can thus be represented by a coherent spin state (CSS), with maximal total spin, but variable rotation angle θ. The analysis of the CSS is based on counting the number of atoms in the level $|1, 0\rangle$. To this end, the atoms in level $|2, 0\rangle$ are removed and the remaining atoms are counted by fluorescence detection in the mMOT. The detection process starts with a strong reduction of the atomic density by switching off one of the two dipole trap laser beams. A σ^+-polarized light push at a magnetic field of 6.7 G accelerates and removes the $F = 2$ atoms from the trap, while the probability of unwanted collisions is reduced by the low density. The removal of atoms in level $|2, 0\rangle$ has a finite extinction ratio of 42.4 dB, resulting in an unwanted, Poisson-distributed remainder of 0.27 atoms maximally. These atoms are produced by two processes: (i) they escape the removal process to the level $F = 1$ because of imperfect optical pumping, and (ii) they are captured from the background gas, which is temporally increased after the operation of the two-dimensional magneto-optical trap. We detect the remaining atoms in the mMOT setup, consisting of a magneto-optical trap with millimeter-sized illumination beams [51,52]. The optical dipole trap is switched off to start an equilibration phase in the mMOT of 50 ms. Subsequently, the main atom counting signal is obtained by collecting fluorescence light for 65 ms with a charge-coupled-device camera. Finally, a second image without atoms is recorded for background subtraction. The spin preparation and detection processes require a total of 1.8 s. After nine measurement runs, the system is halted for 60 s to avoid a slow increase of the mMOT capture rate from the background gas.

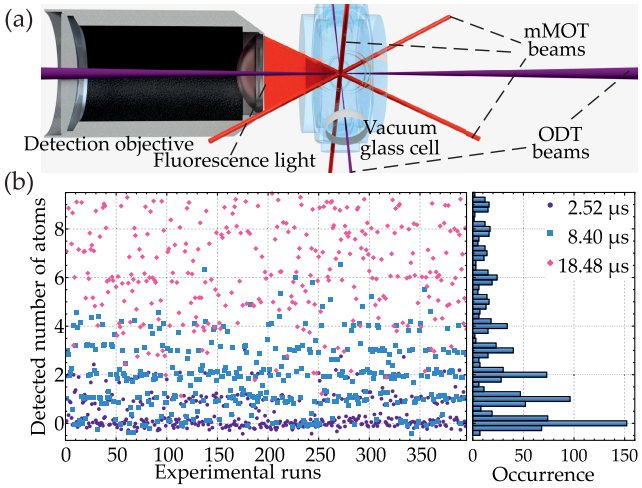

FIG. 1. (a) Sketch of the experimental setup. (b) Time trace of the sequentially measured number of atoms in dependence of the MW pulse length. The number of atoms in $|1, 0\rangle$ after 2.52 μs (dark blue circles), 8.4 μs (blue rectangles), and 18.48 μs (light blue diamonds) is shown for up to 9 atoms for 1106 successive measurements. The accumulation of data points at integer numbers is indicating our number-resolving counting. The histogram of the fluorescence signal on the right further illustrates this effect. Negative values are caused by background substraction.

Figure 1(a) shows a sketch of the experimental setup including the mMOT and ODT beams and the high-numerical-aperture detection objective. Figure 1(b) shows a time trace of 100 consecutive number measurements in $|1, 0\rangle$ for three different MW pulse lengths. The measured number of atoms accumulate at integer numbers, enabling a number assignment fidelity ranging from 99.7% at 1 atom to 99.0% at 15 atoms [52].

Figure 2(a) shows the mean number of the transferred atoms as a function of the microwave pulse duration. The mean atom number follows a sinusoidal Rabi oscillation with a Rabi frequency $\Omega = 2\pi \times 8.2$ kHz (see below). Figures 2(b)–2(e) present the exemplary histograms, which can be associated to rotation angles $\theta = \Omega t$. Without rotation (b), the distribution shows the detection of recaptured atoms, which can be treated as statistical dark counts in the detection system. For finite rotations (c)–(e), the distributions shift to higher atom number and increased width.

Under the assumptions that the microwave generates a homogeneous coupling to the cloud and that level $|1, 0\rangle$ is

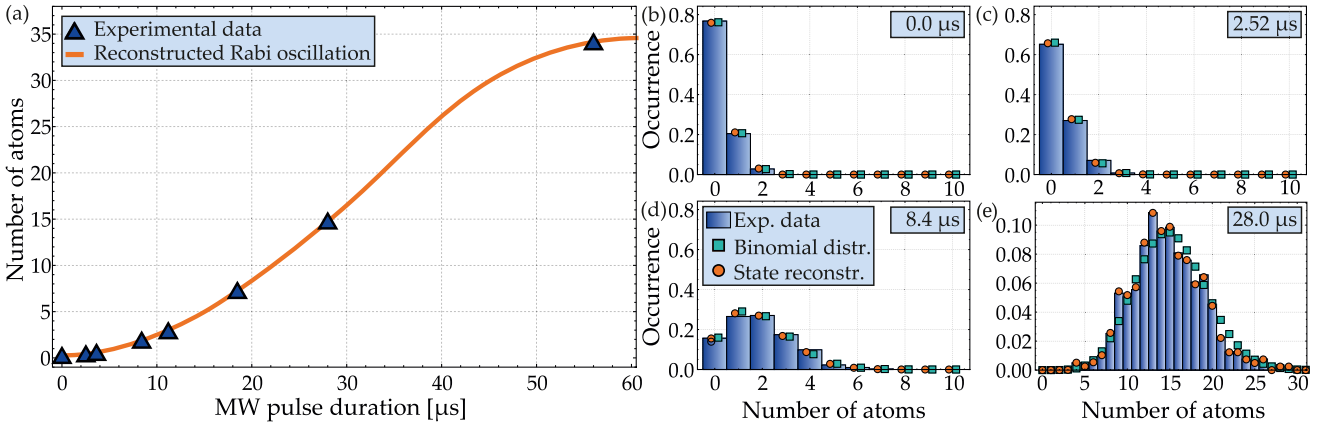

FIG. 2. (a) Mean number of atoms detected in $|1,0\rangle$ in dependence of the MW pulse duration. Each data point (blue triangle) corresponds to an individual atom number distribution. Those are exemplarily shown in the histograms in (b)–(e) for MW pulses ranging from $t = 0$ μs to 28 μs. The ideal binomial distributions accounting for the detection offset and the atom number fluctuations are illustrated in the cyan rectangles. The solid orange line shows the Rabi oscillation with parameters derived from the state reconstruction and the orange circles show the results obtained from the QDT algorithm (see text).

initially completely empty—that are both very well fulfilled in our case—we can use the recorded data for QDT. We associate the two clock levels $|1,0\rangle$ and $|2,0\rangle$ with the letters a and b, respectively, to simplify the notation. We model the detection by expressing the probability of a measurement result n (the number of atoms in clock level a) as

$$P_V(n|t) = \sum_{m=0}^{+\infty} V_{n,m} P_{\mathrm{id}}(m|t), \tag{1}$$

in terms of a stochastic matrix V with non-negative elements $V_{n,m} \geq 0$, which satisfies the normalization property $\sum_n V_{n,m} = 1$ for all m. $V_{n,m}$ can be interpreted as the probability to measure n atoms if m atoms reach the detector. We use the ideal probability $P_{\mathrm{id}}(m|t) = \mathrm{Tr}[|m\rangle\langle m|\hat{\rho}(t)]$, where $\hat{\rho} = \sum_{N=0}^{+\infty} \rho_N |N\rangle_b|0\rangle_a\langle 0|_a\langle N|_b$ is the generic atomic state before starting the dynamics, $\hat{U}(t) = \exp[-i\Omega_R t \hat{J}_x]$ describes the Rabi coupling, $\hat{J}_x = (\hat{a}^\dagger\hat{b} + \hat{a}\hat{b}^\dagger)/2$, $\hat{J}_y = (\hat{a}^\dagger\hat{b} - \hat{a}\hat{b}^\dagger)/(2i)$, and $\hat{J}_z = (\hat{a}^\dagger\hat{a} - \hat{b}\hat{b}^\dagger)/2$ are pseudospin operators, and $\hat{\rho}(t) = \hat{U}(t)\hat{\rho}\,\hat{U}(t)^\dagger$. The assumption that the initial state is diagonal is well justified experimentally. The matrix V provides a full characterization of the detection process, including finite resolutions and biases. It should be noticed that Eq. (1) can be rewritten as $P_V(n|t) = \mathrm{Tr}[\hat{\rho}(t)\hat{\Pi}_n]$, in terms of a POVM set $\{\hat{\Pi}_n\}$, where

$$\hat{\Pi}_n = \sum_{m=0}^{+\infty} V_{n,m} |m\rangle\langle m|. \tag{2}$$

V being positive semidefinite guarantees that $\hat{\Pi}_n \geq 0$, while the condition $\sum_n V_{n,m} = 1$ for all m guarantees the completeness relation $\sum_n \hat{\Pi}_n = \mathbb{1}$.

Our QDT protocol consists of finding the coefficients ρ_N, $V_{n,m}$, and Ω_R that minimize a cost function (see details in the Supplemental Material [53]).

In Fig. 2 we compare the experimental histograms (bars) with the probabilities derived from the QDT (orange circles), namely Eq. (1) with V, ρ_N, and Ω_R calculated using the minimization algorithm. The agreement is excellent, as the obtained probability distribution $P_V(n|t_j)$ achieves a very high fidelity with $P_{\mathrm{exp}}(n|t_j)$, for all t_j (notice that the iterative optimization algorithm is stopped when $\mathcal{C} = 0.01$, which is a value close to saturation [53]). The histograms are consistent with that calculated with a binomial distribution (green squares). The latter assumes a Gaussian distribution of the total number of atoms with measured mean and standard deviation, ideal Rabi transfer, and the convolution with a binomial distribution with a mean number of 0.27 atoms to account for the unwanted detection of background atoms. The mean number of atoms as a function of time, $\sum_n P_V(n,t)n$ for the reconstructed V, ρ_N, and Ω_R interpolates well the detection events as shown in Fig. 2(a). The Rabi frequency extracted from the tomographic reconstruction $\Omega_R = 8.2 \pm 0.2$ kHz agrees with the result of a sinusoidal fit to the data.

In Fig. 3 we show the results of our joint detection and state reconstruction. For most values of m, the weights $V_{n,m}$ [Fig. 3(a)] concentrate around the diagonal $n = m$, where they reach their maximal value. In panel (b) we show $V_{n,m}$ as a function of n and for the specific values $m = 0$ and 5, the histograms are cuts of the plot of panel (a). For $m \gtrsim 20$, the reconstructed $V_{n,m}$ spreads away from the diagonal. Here, the QDT becomes uncertain because the recorded probability distributions do not overlap sufficiently (here for $n \gtrsim 20$) and the optimization method is affected by overfitting of the data [58]. To recognize the overfitting effect, we have performed a "learning test"; see Ref. [53],

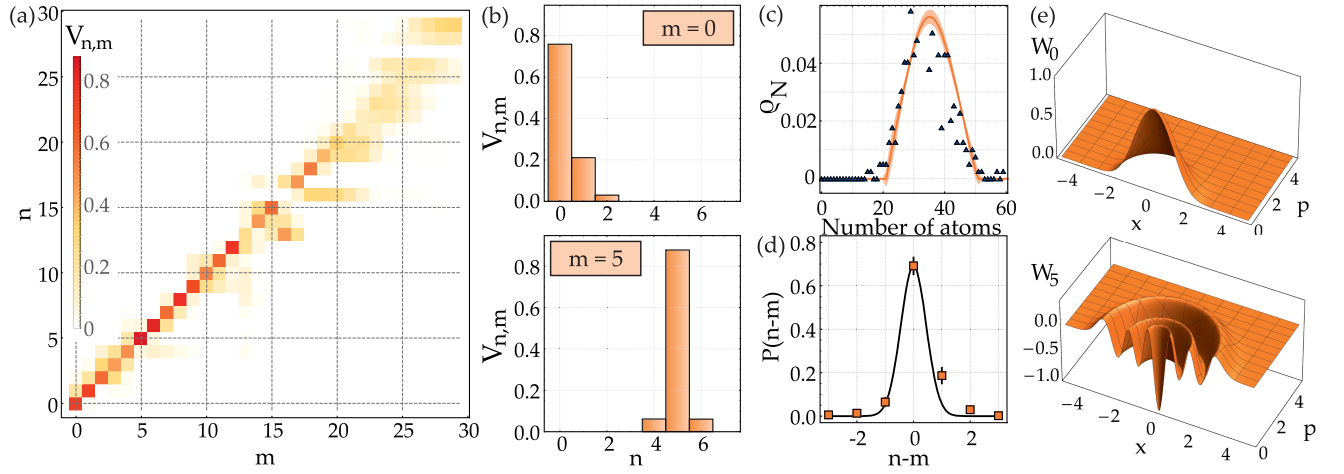

FIG. 3. (a) Reconstructed stochastic map $V_{n,m}$ (linear color scale) as a function of n and m. The highest weight is concentrated along the diagonal $n = m$. (b) $V_{n,m}$ as a function of n and for $m = 0$ and $m = 5$. (c) Coefficients ρ_N of the reconstructed state (orange line with uncertainty shade, see text). The blue triangles show the experimentally obtained state in $|1, 0\rangle$ after a 56 μs MW pulse. (d) $P(n - m)$ as a function of $n - m$ (squares). The black line is a Gaussian fit to the data for $n \leq m$. (e) Wigner function of the POVM operator $\hat{\Pi}_0$ and $\hat{\Pi}_5$, in the (x, p) phase space. Negative Wigner values are observed for $\hat{\Pi}_{n\geq 1}$.

in which the experimental histogram at time t_j is compared with the reconstructed $P_V(n|t_j)$, where the coefficients Ω_R, $\hat{\rho}$, and V are calculated from the minimization algorithm using all of the experimental data except those at time t_j. In this case, we observe a fidelity between $P_V(n|t_j)$ and $P_{\text{exp}}(n|t_j)$ above 99% for times t_j up to 18.48 μs [53]. In the future, a QDT at larger atom numbers can be obtained by taking more histograms with larger statistics. In panel (c) we show the reconstructed elements ρ_N as a function of the number of particles. As we see, the reconstructed diagonal state has approximately a Gaussian shape with mean $\bar{N} = 35.4$ and root mean square error $\Delta\hat{N} = 6.4 \approx \bar{N}^{1/2}$.

For $m \lesssim 20$, $V_{n,m}$ is strongly peaked around $n = m$. It is thus convenient to calculate $P(n - m) = \sum_m V_{n-m,m}P_m$, giving the reconstructed probability that $n - m$ particles are detected if m particles hit the detector. Here, $P_m = \sum_j P_{\text{id}}(m|t_j)$ is the overall probability that m particles hit the detector; it takes into account the most likely detection events and is almost negligible for $m \gtrsim 20$. For a noiseless detector $P(n - m)$ is a delta peak at $n = m$, regardless of the P_m distribution. In our case, $P(n - m)$ is still strongly peaked at $n = m$, with an overall probability of about 70%; see Fig. 3(d). It is remarkable that the recorded broad distributions, which include the effect of number counting noise, are so identical to the theoretically expected distributions, that the QDT unveils the desired high-fidelity counting capability. The slight asymmetry of the distribution V_{n-m} reflects the unwanted recapture of atoms described above, which biases V_{n-m} to positive values of $n - m$. By calculating the variance of the $P(n - m)$ distribution for $n \leq m$ (thus not affected by the atom recapture) we can extract a detection sensitivity $\sigma = 0.4 \pm 0.02$. This counting uncertainty is larger than the uncertainty obtained from Fig. 1, because the finite number of measurements additionally deteriorates the QDT.

As shown in Eq. (2), accessing the matrix V allows us to characterize the POVM elements $\hat{\Pi}_n$. For instance, in Fig. 3(d), we plot the Wigner distribution of the reconstructed POVM operators $\hat{\Pi}_n$ [59]. For $n = 0$ the Wigner function is positive, as expected, corresponding to the detection of vacuum. On the contrary, for $n \geq 1$, the Wigner functions $W_n(q, p)$ have negative values, despite the presence of off-diagonal contributions that indicate the absence of a classical analog of these operators. To emphasize the fundamental quantum nature of our detection we notice that a POVM with negative Wigner function is necessary to prove Bell's nonlocality with Gaussian states (which have positive Wigner distributions) [44,60].

Measuring the atom number in a single level, as demonstrated in our experiment, allows us to surpass the SQL of phase sensitivity in a Ramsey interferometer when using squeezed states. Notice that a single-output-detection Ramsey scheme is analogous to a Michelson-Morley interferometer [61]. The latter is currently exploited in optical gravitational wave detectors, where the SQL has been overcome in prototypes exploiting squeezed-vacuum light [62–65]. The scheme is characterized by a strong asymmetry of output intensity, with most of the particles exiting the undetected mode b. At the optimal value of the interferometer phase shift θ, we predict a phase uncertainty [53]

$$(\Delta\theta)^2 = \frac{\xi_R^2}{\bar{N}} - \frac{\mathcal{C}_z + 2\mathcal{V}_z}{2\langle \hat{J}_z\rangle^2} + \frac{\sqrt{-\mathcal{C}_z}\sqrt{\mathcal{V}_z + \mathcal{V}_N + \mathcal{C}_z}}{\sqrt{2}\langle \hat{J}_z\rangle^2}, \quad (3)$$

where $\xi_R^2 = \bar{N}\mathcal{V}_x/\langle \hat{J}_z\rangle^2$ is the Wineland spin-squeezing parameter [3,66]. Here, $\mathcal{V}_{x,z} = (\Delta\hat{J}_{x,z})^2 = \langle \hat{J}_{x,z}^2\rangle - \langle \hat{J}_{x,z}\rangle^2$ and $\mathcal{V}_N = (\Delta\hat{N}/2)^2$ are variances, $\mathcal{C}_z = \langle \hat{J}_z\hat{N}\rangle - \langle \hat{J}_z\rangle\langle \hat{N}\rangle$ is the covariance, $\hat{N} = \hat{a}^\dagger\hat{a} + \hat{b}^\dagger\hat{b}$ is the number of particles operator, and expectation values are calculated on the probe state of the interferometer. Equation (3) holds when one input (mode b, in particular) is much more populated than the other. Notice that the last two terms in Eq. (3) are not present when measuring both output ports of the interferometer [3,66] and they explicitly depend on the fluctuations of the total number of particles. In particular, for a superposition of coherent spin states with $\langle \hat{J}_z\rangle = -\bar{N}/2$, the last two terms in Eq. (3) vanish and we recover the SQL at the optimal working point $\theta = 0$. For moderate squeezing, $\xi_R^2 \lesssim 1$, the first term in Eq. (3) still dominates and we find $(\Delta\theta)^2 \approx \xi_R^2/\bar{N}$, showing the possibility to achieve sub-SQL sensitivities. Finally, the last two terms in Eq. (3) become relevant for highly spin-squeezed states and thus limit the sensitivity gain due to squeezing. Using a superposition of Gaussian spin-squeezed states, and optimizing the squeezing parameter, we obtain a scaling $(\Delta\theta)^2 \propto \bar{N}^{-5/4}$ [53]. This corresponds to 1.3 dB sensitivity enhancement over the SQL for $\bar{N} \approx 36$, as in our experiment, and can be pushed up to 5 (9) dB when increasing the mean atom number and detecting about 100 (1000) atoms in a single output. As a final remark, we have recently observed that our system can detect up to 700 atoms with single-atom resolution, similar to the reported 1000 atoms in Ref. [40].

In summary, we have employed a number-resolving detector to analyze the dynamics of a coherent spin state derived from an atomic BEC. We have characterized the detection process by the simultaneous reconstruction of the diagonal quantum state and the detector's POVM operators. The latter are characterized by negative Wigner functions, thus unveiling the inherent quantum nature of the detector. In the future, the presented detector and the developed QDT techniques will be directly extended to entangled many-body states, promising the detection of entanglement with unprecedented fidelity in the regime of up to 100 atoms.

This work is supported by the QuantERA grants SQUEIS and MENTA. We acknowledge financial support from the Deutsche Forschungsgemeinschaft (DFG, German Research Foundation), Project ID 274200144-SFB 1227 DQ-mat within the project B01 and Germany's Excellence Strategy, EXC-2123 QuantumFrontiers, Project-ID 390837967. M. Q. acknowledges support from the Hannover School for Nanotechnology (HSN).

*hetzel@iqo.uni-hannover.de

[1] A. D. Cronin, J. Schmiedmayer, and D. E. Pritchard, Optics and interferometry with atoms and molecules, Rev. Mod. Phys. **81**, 1051 (2009).
[2] T. Byrnes and E. Ilo-Okeke, *Quantum Atom Optics, Theory and Applications to Quantum Technology* (Cambridge University Press, Cambridge, England, 2021).
[3] L. Pezzè, A. Smerzi, M. K. Oberthaler, R. Schmied, and P. Treutlein, Quantum metrology with nonclassical states of atomic ensembles, Rev. Mod. Phys. **90**, 035005 (2018).
[4] L. Pezzé and A. Smerzi, Entanglement, nonlinear dynamics, and the Heisenberg limit, Phys. Rev. Lett. **102**, 100401 (2009).
[5] J. Appel, P. J. Windpassinger, D. Oblak, U. B. Hoff, N. Kærgaard, and E. S. Polzik, Mesoscopic atomic entanglement for precision measurements beyond the standard quantum limit, Proc. Natl. Acad. Sci. U.S.A. **106**, 10960 (2009).
[6] M. H. Schleier-Smith, I. D. Leroux, and V. Vuletić, States of an ensemble of two-level atoms with reduced quantum uncertainty, Phys. Rev. Lett. **104**, 073604 (2010).
[7] C. Gross, T. Zibold, E. Nicklas, J. Estève, and M. K. Oberthaler, Nonlinear atom interferometer surpasses classical precision limit, Nature (London) **464**, 1165 (2010).
[8] M. Riedel, P. Böhi, Y. Li, T. Hänsch, A. Sinatra, and P. Treutlein, Atom-chip-based generation of entanglement for quantum metrology, Nature (London) **464**, 1170 (2010).
[9] B. Lücke, M. Scherer, J. Kruse, L. Pezzé, F. Deuretzbacher, P. Hyllus, O. Topic, J. Peise, W. Ertmer, J. Arlt, L. Santos, A. Smerzi, and C. Klempt, Twin matter waves for interferometry beyond the classical limit, Science **334**, 773 (2011).
[10] Z. Chen, J. G. Bohnet, S. R. Sankar, J. Dai, and J. K. Thompson, Conditional spin squeezing of a large ensemble via the vacuum Rabi splitting, Phys. Rev. Lett. **106**, 133601 (2011).
[11] C. D. Hamley, C. S. Gerving, T. M. Hoang, E. M. Bookjans, and M. S. Chapman, Spin-nematic squeezed vacuum in a quantum gas, Nat. Phys. **8**, 305 (2012).
[12] T. Berrada, S. van Frank, R. Bücker, T. Schumm, J.-F. Schaff, and J. Schmiedmayer, Integrated Mach-Zehnder interferometer for Bose-Einstein condensates, Nat. Commun. **4** (2013).
[13] H. Strobel, W. Muessel, D. Linnemann, T. Zibold, D. B. Hume, L. Pezzè, A. Smerzi, and M. K. Oberthaler, Fisher information and entanglement of non-Gaussian spin states, Science **345**, 424 (2014).
[14] O. Hosten, N. J. Engelsen, R. Krishnakumar, and M. A. Kasevich, Measurement noise 100 times lower than the quantum-projection limit using entangled atoms, Nature (London) **529**, 505 (2016).
[15] W. Wasilewski, K. Jensen, H. Krauter, J. J. Renema, M. V. Balabas, and E. S. Polzik, Quantum noise limited and entanglement-assisted magnetometry, Phys. Rev. Lett. **104**, 133601 (2010).
[16] R. J. Sewell, M. Koschorreck, M. Napolitano, B. Dubost, N. Behbood, and M. W. Mitchell, Magnetic sensitivity beyond the projection noise limit by spin squeezing, Phys. Rev. Lett. **109**, 253605 (2012).
[17] W. Muessel, H. Strobel, D. Linnemann, D. B. Hume, and M. K. Oberthaler, Scalable spin squeezing for

quantum-enhanced magnetometry with Bose-Einstein condensates, Phys. Rev. Lett. **113**, 103004 (2014).
[18] C. F. Ockeloen, R. Schmied, M. F. Riedel, and P. Treutlein, Quantum metrology with a scanning probe atom interferometer, Phys. Rev. Lett. **111**, 143001 (2013).
[19] A. Louchet-Chauvet, J. Appel, J. J. Renema, D. Oblak, N. Kjaergaard, and E. S. Polzik, Entanglement-assisted atomic clock beyond the projection noise limit, New J. Phys. **12**, 065032 (2010).
[20] I. D. Leroux, M. H. Schleier-Smith, and V. Vuletić, Orientation-dependent entanglement lifetime in a squeezed atomic clock, Phys. Rev. Lett. **104**, 250801 (2010).
[21] I. Kruse, K. Lange, J. Peise, B. Lücke, L. Pezzè, J. Arlt, W. Ertmer, C. Lisdat, L. Santos, A. Smerzi, and C. Klempt, Improvement of an atomic clock using squeezed vacuum, Phys. Rev. Lett. **117**, 143004 (2016).
[22] E. Pedrozo-Peñafiel, S. Colombo, C. Shu, A. F. Adiyatullin, Z. Li, E. Mendez, B. Braverman, A. Kawasaki, D. Akamatsu, Y. Xiao, and V. Vuletić, Entanglement on an optical atomic-clock transition, Nature (London) **588**, 414 (2020).
[23] F. Anders, A. Idel, P. Feldmann, D. Bondarenko, S. Loriani, K. Lange, J. Peise, M. Gersemann, B. Meyer-Hoppe, S. Abend, N. Gaaloul, C. Schubert, D. Schlippert, L. Santos, E. Rasel, and C. Klempt, Momentum entanglement for atom interferometry, Phys. Rev. Lett. **127**, 140402 (2021).
[24] G. P. Greve, C. Luo, B. Wu, and J. K. Thompson, Entanglement-enhanced matter-wave interferometry in a high-finesse cavity, Nature (London) **610**, 472 (2022).
[25] M. Fadel, T. Zibold, B. Décamps, and P. Treutlein, Spatial entanglement patterns and Einstein-Podolsky-Rosen steering in Bose-Einstein condensates, Science **360**, 409 (2018).
[26] A. Qu, B. Evrard, J. Dalibard, and F. Gerbier, Probing spin correlations in a Bose-Einstein condensate near the single-atom level, Phys. Rev. Lett. **125**, 033401 (2020).
[27] B. Lücke, J. Peise, G. Vitagliano, J. Arlt, L. Santos, G. Tóth, and C. Klempt, Detecting multiparticle entanglement of Dicke states, Phys. Rev. Lett. **112**, 155304 (2014).
[28] X.-Y. Luo, Y.-Q. Zou, L.-N. Wu, Q. Liu, M.-F. Han, M. K. Tey, and L. You, Deterministic entanglement generation from driving through quantum phase transitions, Science **355**, 620 (2017).
[29] F. Laloë and W. J. Mullin, Interferometry with independent Bose-Einstein condensates: Parity as an EPR/Bell quantum variable, Eur. Phys. J. B **70**, 377 (2009).
[30] R. A. Campos, B. E. A. Saleh, and M. C. Teich, Quantum-mechanical lossless beam splitter: Su(2) symmetry and photon statistics, Phys. Rev. A **40**, 1371 (1989).
[31] Z. Y. Ou, J.-K. Rhee, and L. J. Wang, Observation of four-photon interference with a beam splitter by pulsed parametric down-conversion, Phys. Rev. Lett. **83**, 959 (1999).
[32] M. J. Holland and K. Burnett, Interferometric detection of optical phase shifts at the Heisenberg limit, Phys. Rev. Lett. **71**, 1355 (1993).
[33] P. Bouyer and M. A. Kasevich, Heisenberg-limited spectroscopy with degenerate Bose-Einstein gases, Phys. Rev. A **56**, R1083 (1997).
[34] F. Haas, J. Volz, R. Gehr, J. Reichel, and J. Estève, Entangled states of more than 40 atoms in an optical fiber cavity, Science **344**, 180 (2014).
[35] R. Bücker, A. Perrin, S. Manz, T. Betz, C. Koller, T. Plisson, J. Rottmann, T. Schumm, and J. Schmiedmayer, Single-particle-sensitive imaging of freely propagating ultracold atoms, New J. Phys. **11**, 103039 (2009).
[36] R. Lopes, A. Imanaliev, A. Aspect, M. Cheneau, D. Boiron, and C. I. Westbrook, Atomic Hong-Ou-Mandel experiment, Nature (London) **520**, 66 (2015).
[37] C. Carcy, H. Cayla, A. Tenart, A. Aspect, M. Mancini, and D. Clément, Momentum-space atom correlations in a mott insulator, Phys. Rev. X **9**, 041028 (2019).
[38] D. K. Shin, B. M. Henson, S. S. Hodgman, T. Wasak, J. Chwedeńczuk, and A. G. Truscott, Bell correlations between spatially separated pairs of atoms, Nat. Commun. **10**, 4447 (2019).
[39] G. Hercé, J.-P. Bureik, A. Ténart, A. Aspect, A. Dareau, and D. Clément, Full counting statistics of interacting lattice gases after an expansion: The role of condensate depletion in many-body coherence, Phys. Rev. Res. **5**, L012037 (2023).
[40] D. B. Hume, I. Stroescu, M. Joos, W. Muessel, H. Strobel, and M. K. Oberthaler, Accurate atom counting in mesoscopic ensembles, Phys. Rev. Lett. **111**, 253001 (2013).
[41] I. Stroescu, D. B. Hume, and M. K. Oberthaler, Double-well atom trap for fluorescence detection at the Heisenberg limit, Phys. Rev. A **91**, 013412 (2015).
[42] A. Luis and L. L. Sánchez-Soto, Complete characterization of arbitrary quantum measurement processes, Phys. Rev. Lett. **83**, 3573 (1999).
[43] J. Fiurášek, Maximum-likelihood estimation of quantum measurement, Phys. Rev. A **64**, 024102 (2001).
[44] J. Lundeen, A. Feito, H. Coldenstrodt-Ronge, C. Silberhorn, T. C. Ralph, J. Eisert, M. B. Plenio, and I. A. Walmsley, Tomography of quantum detectors, Nat. Phys. **5**, 27 (2009).
[45] L. Zhang, H. Coldenstrodt-Ronge, A. Datta, G. Puentes, J. S. Lundeen, X.-M. Jin, B. J. Smith, M. B. Plenio, and I. A. Walmsley, Mapping coherence in measurement via full quantum tomography of a hybrid optical detector, Nat. Photonics **6**, 364 (2012).
[46] S. Grandi, A. Zavatta, M. Bellini, and M. G. A. Paris, Experimental quantum tomography of a homodyne detector, New J. Phys. **19**, 053015 (2017).
[47] A. Zhang, J. Xie, H. Xu, K. Zheng, H. Zhang, Y.-T. Poon, V. Vedral, and L. Zhang, Experimental self-characterization of quantum measurements, Phys. Rev. Lett. **124**, 040402 (2020).
[48] G. Brida, L. Ciavarella, I. P. Degiovanni, M. Genovese, L. Lolli, M. G. Mingolla, F. Piacentini, M. Rajteri, E. Taralli, and M. G. A. Paris, Quantum characterization of superconducting photon counters, New J. Phys. **14**, 085001 (2012).
[49] A. C. Keith, C. H. Baldwin, S. Glancy, and E. Knill, Joint quantum-state and measurement tomography with incomplete measurements, Phys. Rev. A **98**, 042318 (2018).
[50] Y. Chen, M. Farahzad, S. Yoo, and T.-C. Wei, Detector tomography on IBM quantum computers and mitigation of an imperfect measurement, Phys. Rev. A **100**, 052315 (2019).
[51] A. Hüper, C. Pür, M. Hetzel, J. Geng, J. Peise, I. Kruse, M. Kristensen, W. Ertmer, J. Arlt, and C. Klempt,

Number-resolved preparation of mesoscopic atomic ensembles, New J. Phys. **23**, 113046 (2021).

[52] C. Pür, M. Hetzel, M. Quensen, A. Hüper, J. Geng, J. Kruse, W. Ertmer, and C. Klempt, Rapid generation and number-resolved detection of spinor rubidium Bose-Einstein condensates, Phys. Rev. A **107**, 033303 (2023).

[53] See Supplemental Material, which includes Refs. [54–57], at http://link.aps.org/supplemental/10.1103/PhysRevLett.131.260601 for more details about the optimization algorithm and a detailed analysis about the possibility to reach subshot noise sensitivities.

[54] I. Bengtsson and K. Zyczkowski, *Geometry of Quantum States: An Introduction to Quantum Entanglement* (Cambridge University Press, Cambridge, England, 2006).

[55] L. Pezzè and A. Smerzi, Quantum phase estimation algorithm with Gaussian spin states, PRX Quantum **2**, 040301 (2021).

[56] S. Barnett and P. Radmore, *Methods of Theoretical Quantum Optics* (Clarendon Press, Oxford, 1997).

[57] R. Corgier, M. Malitesta, A. Smerzi, and L. Pezzè, Quantum-enhanced differential atom interferometers and clocks with spin-squeezing swapping, Quantum **7**, 965 (2023).

[58] See for instance M. A. Nielsen, *Neural Networks and Deep Learning* (Determination Press, 2015), http://neuralnetworksanddeeplearning.com.

[59] Explicitly, $W_n(x,p) = \sum_m V_{n,m} W(x,p;m)$, where the Wigner function of the Fock state is $|m\rangle W_n(x,p) = \sum_m V_{n,m}[(-1)^m/\pi] e^{-(x^2+p^2)} L_m[2(p^2+x^2)]$, where $L_m(x)$ denotes the mth Laguerre polynomial.

[60] K. Banaszek and K. Wódkiewicz, Nonlocality of the Einstein-Podolsky-Rosen state in the Wigner representation, Phys. Rev. A **58**, 4345 (1998).

[61] R. Loudon, Quantum limit on the Michelson interferometer used for gravitational-wave detection, Phys. Rev. Lett. **47**, 815 (1981).

[62] J. Abadie *et al.* (LIGO Collaboration), A gravitational wave observatory operating beyond the quantum shot-noise limit, Nat. Phys. **7**, 962 (2011).

[63] J. Aasi *et al.* (LIGO Collaboration), Enhanced sensitivity of the LIGO gravitational wave detector by using squeezed states of light, Nat. Photonics **7**, 613 (2013).

[64] M. Tse *et al.* (LIGO Collaboration), Quantum-enhanced Advanced LIGO detectors in the era of gravitational-wave astronomy, Phys. Rev. Lett. **123**, 231107 (2019).

[65] F. Acernese *et al.* (Virgo Collaboration), Increasing the astrophysical reach of the advanced virgo detector via the application of squeezed vacuum states of light, Phys. Rev. Lett. **123**, 231108 (2019).

[66] D. J. Wineland, J. J. Bollinger, W. M. Itano, and D. J. Heinzen, Squeezed atomic states and projection noise in spectroscopy, Phys. Rev. A **50**, 67 (1994).